Journal of Materials Chemistry

Cite this: J. Mater. Chem., 2012, 22, 25471

www.rsc.org/materials

PAPER

Influence of pH on the fluorescence properties of graphene quantum dots using ozonation pre-oxide hydrothermal synthesis†

Feng Yang,[a] Meilian Zhao,[a] Baozhan Zheng,[a] Dan Xiao,[a] Li Wu*[b] and Yong Guo*[a]

Received 13th August 2012, Accepted 19th October 2012
DOI: 10.1039/c2jm35471c

Recent research into graphene-based materials is largely focused on graphene quantum dots (GQDs) and their optical properties. A facile method has been developed to extract GQDs from reduced graphene oxide (RGO) by the ozonation pre-oxide method. The as-prepared GQDs, which were 2–5 nm in diameter, exhibited strong fluorescence activity ranging from ~355 nm to ~440 nm. The prepared GQDs possessed strong fluorescence with quantum yields from 3.18% to 9.48%. What's more, the fluorescence properties of the GQDs could be determined by tuning the pH of the ozonation system. We speculated the mechanisms of ozonation, thermal and hydrothermal treatment. We found that pyrocatechol could lead to fluorescence quenching of the GQDs, which might produce novel potential for the detection of targets.

1. Introduction

In recent years, graphene which was discovered by Geim[1] has attracted both theoretical and experimental scientists, as this material exhibits excellent mechanical properties, high ballistic conductivity, high elasticity, and good electrical properties resulting from its atomic thickness and its two-dimensional crystal with carbon atoms arranged in a honeycomb lattice.[2–4] Graphene oxide (GO), a precursor of graphene, is an interesting material. Recently, carbon quantum dots (CQDs) made directly from activated carbon[5] or other carbon targets[6] have been widely investigated for their intrinsic properties, such as chemical inertness, biocompatibility, water dispersibility, low toxicity and easy labeling in biological and biomedical fields. Thus, they attract more and more attention with the emergence of carbon nanotubes, fullerenes, and graphene.[6–16]

Much research has been concerned with the properties and applications of graphene quantum dots (GQDs), especially their synthesis methods. Hence, several effective techniques have been developed for preparation. The main synthesis approaches focus on chemical methods.[6,16] Chemical approaches are quite attractive because (1) it directly induces oxygen functionalization to the carbon source which means that oxygen-containing groups can be used as reactive sites when applied to other fields, and (2) by careful selection of the methods and surface modifier, better control of size, shape and physical properties is possible. Physical approaches are limited by the experimental cost and difficulties in obtaining smooth edges, while chemical routes can overcome these drawbacks. The chemical approaches mainly focus on two strategies: "bottom-up" chemical synthesis[17,18] and "top-down"[13,15,19,20] by cutting the carbon resource.

The properties of GQDs are substantially different from reduced graphene oxide (RGO), due to the defects in the basal plane and the quantum size effects caused by hydrothermal cutting. Compared with chemical reduction,[21,22] solvent-assisted thermal reduction[23,24] or electrochemical reduction,[25,26] thermal treatment[27] can reduce GO (micro-scale) to RGO with small size (nano-scale). The pre-oxidation is the key to hydrothermal synthesis of GQDs, because it introduces oxygen-containing groups and defects at edges and in the basal plane as reactive sites. However, the traditional chemical methods, which introduce many strong oxidizing acids in complicated operations, are time-consuming and it is difficult to control the degree of oxidation of RGO in the synthesis of GQDs with certain optical properties. The acidic oxidizing agents (*e.g.* H_2SO_4 and HNO_3)[13,28] usually need a long-time procedure (about 10–24 h). Recently, due to the high oxidative capability of ozone, it has been known to react with single-walled nanotubes (SWNTs)[11] and fullerene[12,29] to form nano-size fragments with a series of oxygen-containing functional groups. Several teams have studied the electronic and transport properties of graphene after functionalization *via* ozone treatment,[30] and the physical process of adsorption of ozone on graphene.[31] But little was about using ozone as the oxidizing agent in RGO synthesis. In this work, we took advantage of the high oxidative capability of O_3 (g) as a pre-oxidizing agent to obtain ozonized products (O-RGO) in synthesizing GQDs with different fluorescence properties.

The fluorescence of GQDs was found to be in the near-infrared (IR) and visible (vis) wavelength range when excited with

[a]College of Chemistry, Sichuan University, Chengdu, 610064, P. R. China. E-mail: guoy@scu.edu.cn; Fax: +86-28-85412907; Tel: +86-28-85416218
[b]Analytical & Testing Center, Sichuan University, Chengdu, 610064, P. R. China. E-mail: wuli@scu.edu.cn; Fax: +86-28-85412316; Tel: +86-28-85412956

† Electronic supplementary information (ESI) available: Morphology of precursors; morphology of GQDs and the probable mechanism for fluorescence quenching. See DOI: 10.1039/c2jm35471c

ultraviolet radiation, a property useful for biosensing and fluorescence tags.[4,15,20,32] However, production and extensive applications are hindered by effective control of the oxidation degree and groups in the RGO. Hence, it is significantly valuable to develop more effective GQD synthesis methods.

In this research, we chose the ozonation pre-oxide hydrothermal method as a model system, and investigated the relationship between the pH of the ozonation pre-oxide hydrothermal method and the fluorescence properties. It is noted that the ozonation pre-oxide method is simple and efficient, low-cost, massively scalable and well controllable to obtain GQDs with different fluorescence properties. Hopefully, not only can this investigation of GQDs be valuable in facilitating the synthesis process, but also we can gain a good understanding of these versatile materials. What's more, this work would inspire broader interests and stimulate more exciting developments in the promising fluorescence field of research.

2. Experimental section

2.1. Materials

All chemicals used were of analytical grade. Graphite powder (spectral pure, Shanghai Huayi Company, China). Hydrogen peroxide (H_2O_2, 30%) was bought from Guangdong Chemical Reagent Engineering-Technological Research and Development Center (Guangdong, China). Phosphorus pentoxide (P_4O_{10}), sodium hydroxide (NaOH, >99%), sulfuric acid (H_2SO_4, 98%), and potassium permanganate ($KMnO_4$, >99.5%) were obtained from Kelong Technological Co. (Chengdu Sichuan, China). Potassium peroxydisulfate ($K_2S_2O_8$, >99.5%) was purchased from Sinopharm Chemical Reagent Co. (Sichuan, China). Quinine sulfate (99%) was purchased from J&K Chemical Ltd. (Beijing, China). All chemicals were used as received without further purification, and all solutions were prepared freshly daily in pure water. The water used in the experiments was freshly deionized using an ultrapure water system.

2.2. Instruments

High resolution transmission electron microscopy (HR-TEM) and scanning transmission electron microscopy (STEM) observations were performed with one drop of the aqueous nanosheet suspension deposited on a holey carbon film on a TECNAL G2 F20 (bought from FEI company) electron microscope operating at 200 kV. X-Ray diffractions (XRD) were obtained with a Tongda TD-3500 X-ray powder diffractometer (Liaoning, China) using Cu Kα radiation ($\lambda = 0.154$ nm). The XRD patterns were recorded from 5° to 60° with a scanning rate of 0.03° s^{-1}. All Raman spectra were collected on a Lab RAM HR with a 785 nm wavelength laser (HORIBA Jobin Yvon S.A.S.). Samples were scanned from 1000 to 2000 cm^{-1} to visualize the D and G bands. Spectra were collected with a 5 s exposure time. Absorption spectra were recorded at room temperature on a U-1100 UV-vis spectrophotometer. Fluorescence measurements were done with a F-7000 Hitachi spectrometer. Fluorescence experimental conditions: the photomultiplier tube (PMT) voltage was set at 700 V, and the slit widths for excitation and emission were 2.5 nm and 5.0 nm, respectively. Fourier transform infrared spectroscopy (FT-IR): KBr and samples were dried under vacuum and then scanned from 4000 cm^{-1} to 750 cm^{-1} on a FT-IR spectrometer system (NICOLET-6700). X-Ray photoelectron spectroscopy (XPS) spectra of the samples were measured by a Kratos XSAM800 system taking Al as the source for determining the composition and chemical bonding configuration.

2.3. Experiments

GO was prepared from graphite powder that underwent a pre-oxidation step by a modified Hummers' method.[2] GO was formed from graphite oxide which was diluted to 1 : 6 with double deionized (DI) water and exfoliated for 1 h using an ultrasonic homogenizer. The obtained brown dispersion (GO) was subjected to 20 min of centrifugation at 5000 rpm to remove unexfoliated graphite oxide, and then 20 min of centrifugation at 1200 rpm to remove some other impurities and metal ions. GO was re-oxidized employing hydrogen peroxide and ozone to form ozonized graphene oxide (O-GO). GO dispersed in deionized (DI) water with hydrogen peroxide (0.05 mL) at pH 2.0 water solution. Then, the mixture was treated for 1 h with ozone. The ozone, which was generated by an OZ-7G Ozone Generator, was bubbled through the suspension (dried and clean air as oxygen source). The RGO sheets were obtained by thermal deoxidization of O-GO sheets in a tube furnace at 300 °C for 3 h at a heating rate of 5 °C min^{-1} in argon atmosphere.

RGO (0.01 g) was dispersed in deionized (DI) water (40 mL) at pH around 2.0. The mixtures were ultrasonicated for 1 h, completely dispersing and forming a black suspension system. To those mixtures ozone was introduced for 8 h in an ice-bath and treated for 30 min under violent ultrasonication to obtain ozonized RGO (O-RGO) dispersed solution. The suspension was directly transferred to a poly(tetrafluoroethylene) (Teflon)-lined autoclave (50 mL) and heated at 200 °C for 10 h. After cooling to room temperature, the resulting orange or gray suspensions (black particles existing in some) were filtered through a 0.22 μm microporous membrane and the separated filter solutions were named GQD1.

A series of parallel experiments were implemented as shown in Table 1. The pH values were tuned by either HNO_3 or NaOH. All the solid samples in the account were dried at <50 °C in a vacuum oven.

Table 1 The synthesis conditions for the GQDs[a]

Name	pH of ozonation	pH of hydrothermal treatment	Emission peak
GQD1	~2.0	<1.0	410–425 nm
GQD2	~13.0	<1.0	355–370 nm
GQD3	~2.0	~13.0	420–440 nm
GQD4	~7.0	~13.0	410–430 nm
GQD5	~10.0	~13.0	370–375 nm
GQD6	~13.0	~13.0	370–385 nm

[a] GQDs were obtained at different pH. RGO sheets were treated with ozone in water solution with pH ~ 1.0, 13.0, respectively. They were hydrothermally treated in acidic solutions (pH < 1.0, after ozonation pre-oxide the acidity of solutions was greatly lessened and the pH of solutions was less than 1). GQD3, GQD4, GQD5, GQD6 were treated with ozone in water solutions with pH ~ 2.0, 7.0, 10.0, 13.0, respectively. They were hydrothermally treated at pH ~ 13.0 in aqueous solution.

3. Results and discussion

We employed the modified Hummers' method, which is widely used to prepare GO to introduce oxygen-containing functional groups into graphite sheets. The details were given in the Experimental section. The photographs of the GO and O-GO solid samples and suspensions were shown in Fig. 1a and b and the corresponding insets. GO, O-GO, and RGO showed a series of markedly varied morphologies. The thermal stability, structure and element ratio of GO, O-GO and RGO were characterized by XRD, FT-IR, XPS and TG (Fig. S1 and S2†). The reaction mechanisms were shown in Schemes 2–5. The pH of the reaction media during the ozonation pre-oxide and hydrothermal treatment exerted a drastic influence on the optical properties of the GQDs (see Fig. 8). The changes of fluorescence intensity produced a novel method for the detection of pyrocatechol (Fig. 11).

3.1. Characterization

3.1.1. Precursor. The surface morphologies of GO were enormously changed after ozonation (O-GO) and thermal reduction treatment (RGO) (see Fig. 1). With the extension of the ozonation time, the solution color changed from brown to yellow (insets of Fig. 1a and b). As shown in Fig. S1,† the surface functional groups and interlayer spacing also enormously changed after ozonation (O-GO) and thermal reduction (RGO) (see Fig. S1†). As a nonstoichiometric compound, the specific synthetic process strongly affects the chemical structure of GO. The O-GO sheets were ultrathin with fewer ripples than the GO. The transparency revealed that the O-GO sheets were fully extended with only a few layers. As a result of re-oxidation *via* ozonation, carboxylic and ketone groups were formed to increase the interlayer spacing of O-GO. It was better peeled into fewer layers than GO. The functional groups on the basal plane and at the edges of GO and O-GO substantially influenced the properties of graphene-based materials. Yim and Johnson[11] demonstrated that carbonyl, carboxyl and ester groups on SWNTs evolve CO_2 and CO *via* breaking of the C–C, C–O bonds and creating defects. That is to say, the oxygen groups create defects as chemically reactive sites to make O-GO into a thermally-reduced black powder (RGO) of small size (see Fig. 2). It is an advantage of employing the O-GO as the precursor to synthesize RGO. More details were given in the ESI.†

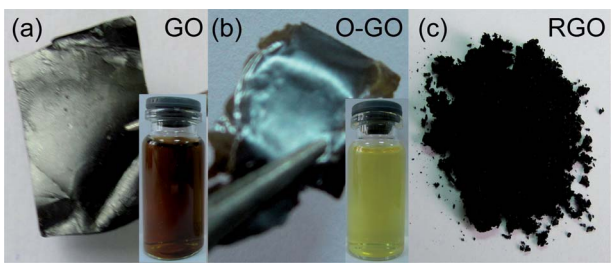

Fig. 1 Photographs of GO (a), O-GO (b), RGO (c) taken under visible light. The inset in panel (a) is a photograph of the GO dispersed system (0.5 mg mL^{-1}) in water and in panel (b) is a photograph of the O-GO (0.5 mg mL^{-1}) solution under visible light.

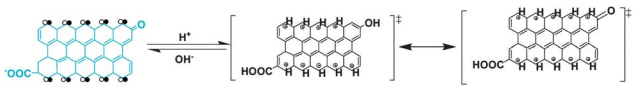

Scheme 1 Models of GQDs in acidic (right) and alkaline (left) media, having surmised from Fig. 8a that the two models of GQDs can be switched mutually in solution depending on pH (• and ○ represent σ electrons and π electrons).[13]

The reactions of O-GO with large amounts of oxygen groups can lead to decomposition by forming CO_2, CO and water vapour during thermal treatment. A series of more marked changes took place after the thermal treatment of the O-GO at 300 °C and the size of the RGO decreased dramatically down to 20–50 nm (see Fig. 2c). Further details can be obtained in the ESI.†

The C 1s XPS has been used to determine the effects triggered by the pH during ozonation on the functional groups of ozonized RGO. As shown in Fig. 3 and S2c,† the percentage of the C=C (~284.5 eV) band decreased from 76.38% (RGO) to 57.78% for O-RGO1 at pH = 2.0 and to 52.66% for O-RGO2 at pH = 13.0. The functional groups depended on the pH during ozonation, such as C–O (~286.5 eV, O-RGO1: 27.56%; O-RGO2: 25.08%), C=O (~287.8 eV, O-RGO1: 9.02%; O-RGO2: 13.88%), and O–C=O (~289 eV, O-RGO1: 5.77%; O-RGO2: 8.38%). That diversity seemed to confirm that pH can affect the efficiency of the ozonation. It demonstrated the successful incorporation of oxygen functional groups into the RGO by controlling the ozonation environment. According to the discussion above, we proposed the probable mechanisms for the ozonation in acid–base systems (see Schemes 3 and 4).

3.1.2. GQDs. Fig. 4 shows the typical HR-TEM and STEM images of GQD1. GQD1 was distributed with diameters in the range of 2–5 nm, forming near circle-like entities

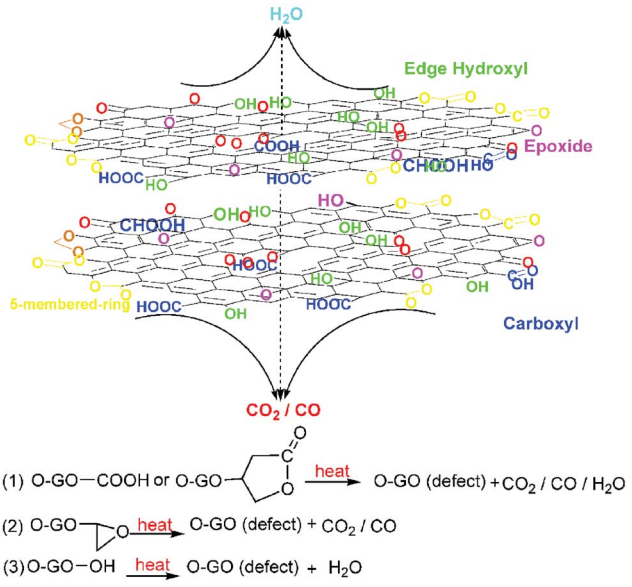

Scheme 2 Mechanism of the deoxidization reaction in a tube furnace with argon gas as protection. Some oxygen containing groups including epoxy, hydroxy, carboxyl groups and carbonyl pair groups, and some carbon–carbon bonds (C–C, C=C) are cut into complete fragments by releasing CO or CO_2 under the thermal treatment.

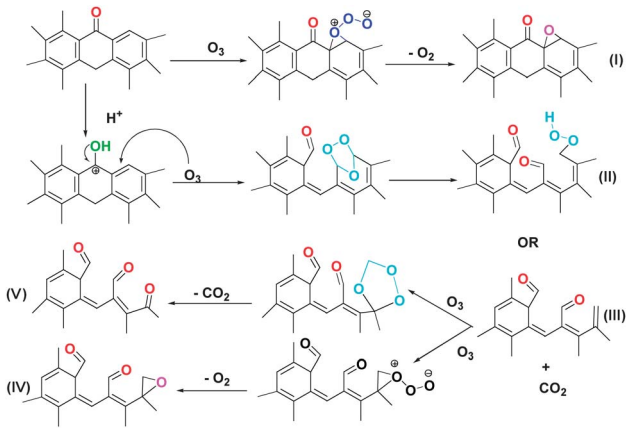

Scheme 3 Mechanism of the ozonation in acidic system. Hydroxy and epoxy groups were the main groups at slow reaction rate in an acidic system.

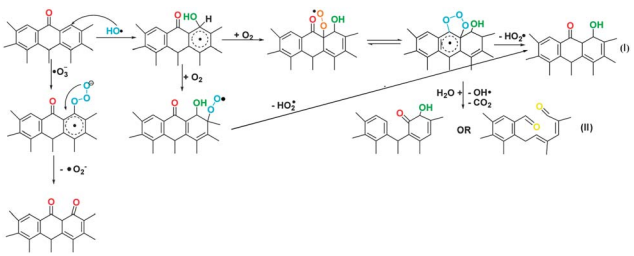

Scheme 4 Mechanism of the ozonation pre-oxide in alkaline system. Dissolved ozone in water is initiated by OH^- under alkaline conditions.

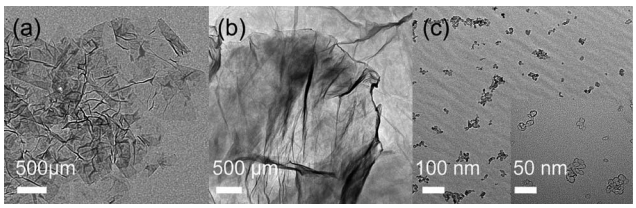

Fig. 2 TEM images of GO (a), O-GO (b) and O-RGO (c) dispersed in water.

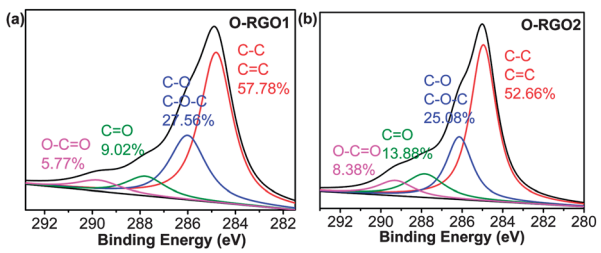

Fig. 3 High-resolution C 1s XPS spectra of (a) O-RGO1 (pre-oxidation at pH = 2.0, in ice-water bath); (b) O-RGO2 (pre-oxidation at pH = 13.0, in ice-water bath).

and mostly monodispersed dots. This result indicated that we prepared GQDs with strong and steady fluorescence *via* a simple, efficient, low-cost and well-controlled route. In order to explore the relationships among pH value, sizes of GQDs and fluorescence properties, we took HR-TEM images of GQD2–GQD6 (see Fig. S3†). The HR-TEM images showed that the GQDs (GQD3–GQD6) were distributed with diameters in the range of 3–5 nm with discernible lattice structures (see Fig. S3†). It can be concluded that the sizes of the GQDs did not conspicuously change regularly with pH value changes.

To characterize graphene-based materials, the Raman technique is a practical method. As shown in Fig. 5, the I_D/I_G ratio was used to evaluate the different structures of the GQDs. The G band is associated with E_{2g} vibrational modes of the aromatic domains, and the D band arises from the breathing modes of the graphitic domains.[33] Traditionally, the I_D/I_G ratio was used to compare the structural order between nanocrystalline and amorphous graphitic systems. The increase of the I_D/I_G ratio sometimes indicated the decrease of the topological disorder in the graphite layer and the increase in the size of nanocrystalline graphite.[23] Paredes *et al.*[34] demonstrated that the I_G/I_D ratio was employed to estimate the average size of C sp^2 domains and Bosch-Navarro[24] employed it to characterize the degree of reduction of GO. As shown in Fig. 5, the I_D/I_G ratios were 1.27, 1.17, 1.36, 1.37, 1.47 and 1.48 for GQD1–GQD6, respectively. There were two possible explanations for the increase in the I_D/I_G ratio. Firstly, the increase of the I_D/I_G ratio indicated the decrease of the fraction of sp^2 domains and different degrees of GQD oxidation.[34] Secondly, there was an increase in the number of defect sites, which were created during the hydrothermal treatment.[23]

Fig. 6 shows the high-resolution XPS spectra (C 1s) of GQD1–GQD6. Comparing the sp^2 (C–C) domains with the sp^3 (C–O) domains (Fig. 6), it confirmed that the number of defects increased during the hydrothermal cutting in basic system. That tendency seemed to confirm that, besides affecting the morphology of the GQDs, the pH of the hydrothermal system also affected the fraction of the sp^2 domain and the oxidation percentage. That was consistent with the results of Raman. It was worth noting that the carbonyl groups (~287.5 eV) of GQD3 and GQD4 disappeared and the oxygen proportions of GQD3–GQD6 were higher than for GQD1 and GQD2. It was speculated that ketone (–C=O) groups were attacked by Ḣ or ȮH at different pH values during hydrothermal treatment. Hence, the possible mechanisms were proposed in Scheme 5.

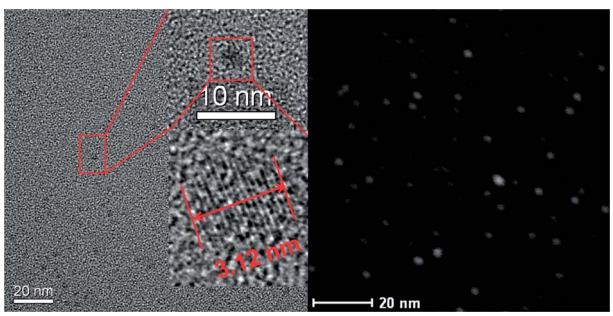

Fig. 4 HR-TEM (a) and STEM (b) images of the aqueous-dispersible GQD1. Insets are the zoomed-in figures of one dot (upper) and the crystalline phase of the dot (lower).

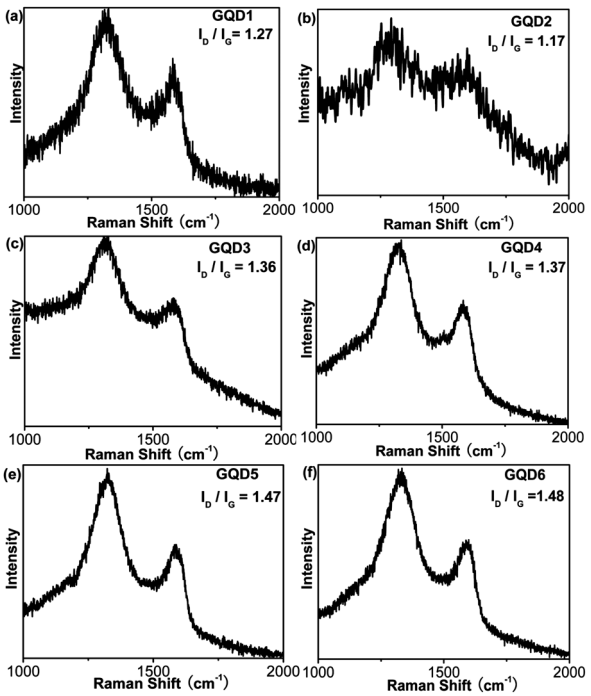

Fig. 5 Raman spectra of GQD1 (a), GQD2 (b), GQD3 (c), GQD4 (d), GQD5 (e), and GQD6 (f) located on a Si/SiO_2 substrate. All the Raman spectra were taken at a laser power of about 4.0 mW and a short collection time of 5 s.

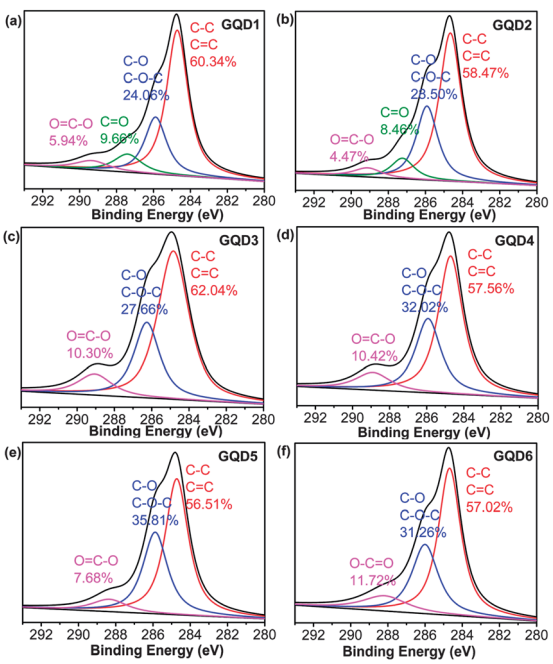

Name	GQD1	GQD2	GQD3	GQD4	GQD5	GQD6
O%	14.95%	15.58%	27.32%	24.81%	21.86%	17.01%

Fig. 6 High-resolution C 1s XPS spectra of GQD1–GQD6. All the GQDs were dried at 45 °C in a vacuum oven for three weeks. The proportion of oxygen in the GQDs was listed below.

3.2. Optical properties

3.2.1. GQD1 synthesized in acidic system. The fluorescence intensity of GQD1 was strong and visible with unaided eyes, which represented the absorption energies corresponding to the emission of blue light. In this section, RGO was pre-oxidized in an acidic system (pH $\sim$ 2.0).

Absorption traces between 230 and 350 nm for the GQD1 suspensions showed no clear features except for a peak near 270 nm originating from a π–π^* transition of the C=C band (see Fig. 7b). The exciton peaks were assigned to a π–π^* transition of the C=C of the as-synthesized GQDs occurring at $\sim$245 nm. The emission peaks around 320 nm were attributed to n–π^* transitions of C=O.[20,24]

The fluorescence intensity of GQD1 was pH-dependent (see Fig. 8). As pH increased, we observed a monotonic increase of the emission intensity without a significant change in shape (Fig. 8a). GQD1 emitted strong fluorescence in alkaline system, while it sharply decreased when the pH was lowered to 7.0. If pH is switched between 13.0 and 1.0, the fluorescence intensity varies reversibly, similar to spectra reported previously.[13] There are several mechanisms to explain the fluorescence of GQDs, such as the triplet ground state theory[13,35,36] and islets theory.[20] However, the mechanism responsible for fluorescence in GQDs, especially shifts to ultraviolet emission, remains to be elucidated. The chemical nature of the zigzag edge sites of graphene-based materials are carbene-like, with a triplet ground state. Not only is this consistent with the key electronic properties and surface activity behavior of carbons, but the triplet ground state can also explain why the fluorescence from the GQDs is pH-dependent (Fig. 8a). As shown in Scheme 1, the possible mechanism of pH-dependent fluorescence was proposed. The fluorescence spectrum of GQD1 was generally broad and depended on the excitation wavelengths (see Fig. 8b). When the excitation wavelength was changed from optimum excitation to longer wavelength in 5 nm steps, the fluorescence peak shifted to longer wavelengths, which was consistent with fluorescent carbon nanoparticles.[10,13,19,20]

3.2.2. The GQDs synthesized in parallel experiments. To test the influence of the pH of the synthesis system on the fluorescence properties of the GQDs, we synthesized GQD1–GQD6 and investigated their photoluminescence properties using absorption and fluorescence spectra.

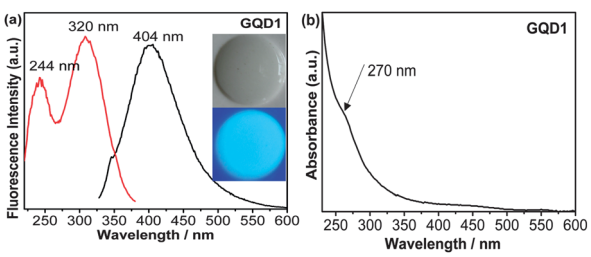

Fig. 7 Fluorescence excitation (red line) and emission (black line) spectra (a) and UV-vis absorption (b) of GQD1 dispersed in water. The inset in panel (a) was the photograph of GQD1, which was taken under visible light (upper) and UV light at 254 nm (lower), respectively.

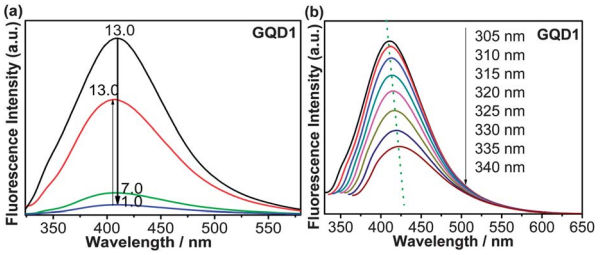

Fig. 8 Fluorescence spectra of GQD1 (a) in water solution when pH was shifted between 1.0 and 13.0. Fluorescence emission spectra of GQD1 (b) were excited at progressively longer excitation wavelengths from the best exciting light on the left in 5 nm increments in aqueous solution.

The fluorescence intensity of the GQDs was strong and visible by unaided eyes under UV light, while some were not visible by naked eyes because the emission peaks shifted to near-ultraviolet (see Fig. 9). Excitation wavelengths between 290 nm and 360 nm (3.4–4.4 eV) represent the absorption energies corresponding to emission of blue light. The corresponding fluorescence spectra of the GQDs synthesized under different acid–base media were shown in Fig. 10a and b.

The emission and absorption spectra of the GQDs were also measured and shown in Fig. 10. With the increase of pH during ozonation, the fluorescence of the obtained GQDs showed a blue shift (see Fig. 10a and b). In contrast to the broad absorption features, relatively narrow fluorescence peaks and their emission peaks ranging from ~440 nm to ~355 nm were observed. The GQDs emitted strong fluorescence in the solution-like suspension, and they covered the visible wavelength range and extended into the near-ultraviolet (Fig. 10a and b). Using quinine sulfate as reference, the fluorescence quantum yields of GQD1–GQD6 were measured to be 6.83%, 4.23%, 6.55%, 3.18%, 9.48% and 7.20%, respectively. The method used to detect the quantum yields of the GQDs was referenced to Grabolle *et al.*[37]

As shown in Fig. 10c, the absorption of GQD1 and GQD2 showed typical absorption peaks at ~270 nm attributed to π–π*

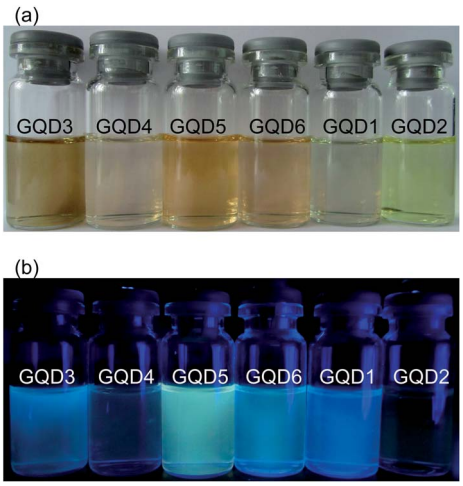

Fig. 9 Photographs of GQD1, GQD2, GQD3, GQD4, GQD5 and GQD6 dispersed in water then filtered through a 0.22 μm microporous membrane taken under (a) visible light and (b) UV light with wavelength of 254 nm, respectively.

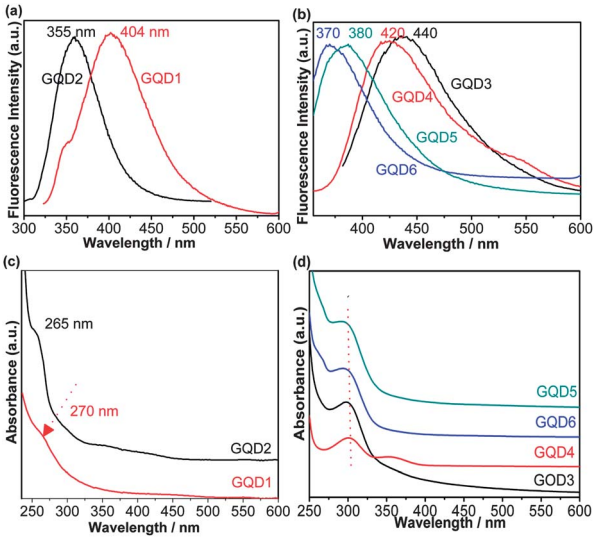

Fig. 10 Fluorescence spectra (a and b) and UV-vis absorption (c and d) of the GQDs (GQD1, GQD2, GQD3, GQD4, GQD5, GQD6) dispersed in water.

transitions of C=C sp^2 domains.[13,20,38] GQD3–GQD6 in solution showed an absorption band centered at ~300 nm (see Fig. 10d), which was consistent with that reported previously.[6,13,20] The main absorbance peaks attributed to n–π* transitions of O=C in the as-synthesized GQD3–GQD6 occurred at around ~300 nm. The two electronic transitions which were observed at ~300 nm (3.81 eV) observed in the absorption spectra of the GQDs can be attributed to transitions from σ and π orbitals, *viz.* highest occupied molecular orbital (HOMO) to lowest unoccupied molecular orbital (LUMO). The absorbance peaks were found to shift with different conditions, which is most likely due to the variation of carboxyl groups, which was consistent with the results of XPS spectra (Fig. 6).

In summary, it was indicated that the oxygen-containing functional groups were influenced by the pH of solution during hydrothermal treatment. It should be noted that the fluorescence peaks shifted to shorter wavelength with the increase of pH from ~2.0 to ~13.0 during ozonation, whether the pH of hydrothermal synthesis was acidic or alkaline.

3.3. Mechanisms

As discussion in Section 3.1, the thermal reduction processes exerted a drastic influence on the morphology (Fig. 1c) and sizes (Fig. 2) of the resulting materials. It can be surmised that CO_2, CO and H_2O molecules are released from the decomposition of epoxy groups, hydroxy groups, carboxylic groups and ketone groups.[39,40] The CO_2 and CO evolution reaction, results in formation of many fragment sheets. That was consistent with the experimental results of TEM and TG (Fig. 2 and S1c†). Boukhvalov and Katsnelson[41] modeled the effect of oxygen and hydroxyl groups on the structure of graphene oxide. They predicted that the carbon–carbon bond length was highly dependent on the types of functional groups and their coverage. As mentioned above, we speculated the probable thermal treatment mechanism in a tube furnace as shown in Scheme 2.

As is well-known, the ozonation mechanism is complex and many groups focus on it. There are two forms of ozone (dissolved ozone or HO· radicals) in acid–base aqueous solution.[42,43] We proposed the probable mechanisms, including direct reaction and indirect reaction with RGO. In the aqueous phase, those reactions processed between RGO and dissolved ozone or HO· radicals. The XPS C 1s (Fig. 3) can be well understood based on the proposed mechanisms (see Scheme 3 and Scheme 4‡).

In acidic system, the dissolved ozone directly reacted with RGO, while ozone was much less reactive than HO·. So it slowly reacted with RGO when the concentration of OH^- was low. The ozonation mechanism was illustrated in Scheme 3.

In alkaline medium, HO· rapidly reacted with reactive sites in the RGO sheets. The HO· radicals are much more reactive than ozone.[44] It reacts much more rapidly than dissolved ozone with RGO. Dissolved ozone is initiated by OH^- in water under alkaline conditions. The chain-reactions of ozone with HO^- are as follows:

$$O_3 + OH^- \rightarrow HO_2^{\cdot} + {}^{\cdot}O_2^- \quad (1)$$

$$HO_2^{\cdot} \rightarrow H^+ + {}^{\cdot}O_2^- \quad (2)$$

$$O_3 + {}^{\cdot}O_2^- \rightarrow {}^{\cdot}O_3^- + O_2 \quad (3)$$

$${}^{\cdot}O_3^- + H_2O \rightarrow OH^{\cdot} + OH^- + O_2 \quad (4)$$

Summarizing, these reactions may be written as:

$$O_3 + OH^- \rightarrow {}^{\cdot}O_3^- + {}^{\cdot}OH$$

Reaction (1) is the chain-initiating step. Its actual free energy will be largely decreased, since the steady state concentrations of HO· and $HO_2^{\cdot}$ will be very small. The result of (3) is the chain decomposition of ozone. Similarly, (3) and (4) constitute a chain process for reaction. The ozonation is a 1e reaction of each free radical with HO·, as the most powerful and reactive oxidizing agent in the system. The conversion of the new radical into a stable product completes the chain breaking process. Furthermore, ozonation reactions are highly exothermic, with weakly bound and reactive intermediates among the initial reaction products. However, different reaction routes have been proposed for the reaction of HO· with RGO to form oxygen-containing functional groups. As shown in Scheme 4, the ozonation reactions formed oxygen-containing functional groups (epoxy, hydroxy, carboxylic and ketone groups) and defects due to breaking the carbon–carbon bonds (in the form of CO or CO_2) from the basal plane (such as Scheme 4(II)). Those made RGO form many fragment sheets (O-RGO). In summary, those mechanisms explained the ozonation with reactive sites in the RGO to form oxygen groups, which were consistent with the XPS results (Fig. 3).

Based on a theory and literature survey, we proposed the hydrothermal treatment mechanism in a poly(tetrafluoroethylene) (Teflon)-lined autoclave (50 mL) as shown in Scheme 5. The –OH, C–O–C, –C=O, and –COOH located in the sheets of O-RGO reacted with HO· or H· and released CO_2, CO, and H_2O, ultimately. Carbon–carbon bonds (C–C) were broken, releasing the strain of the lattice and formed carbonyl groups through ozonation.[45] Carbon–carbon bonds and carbon–oxygen bonds were broken, releasing CO and CO_2 by hydrothermal treatment[13,46] to form GQDs. The conceivable mechanism was identical with the results that the GQDs' fluorescence peaks and absorption were pH-dependent.

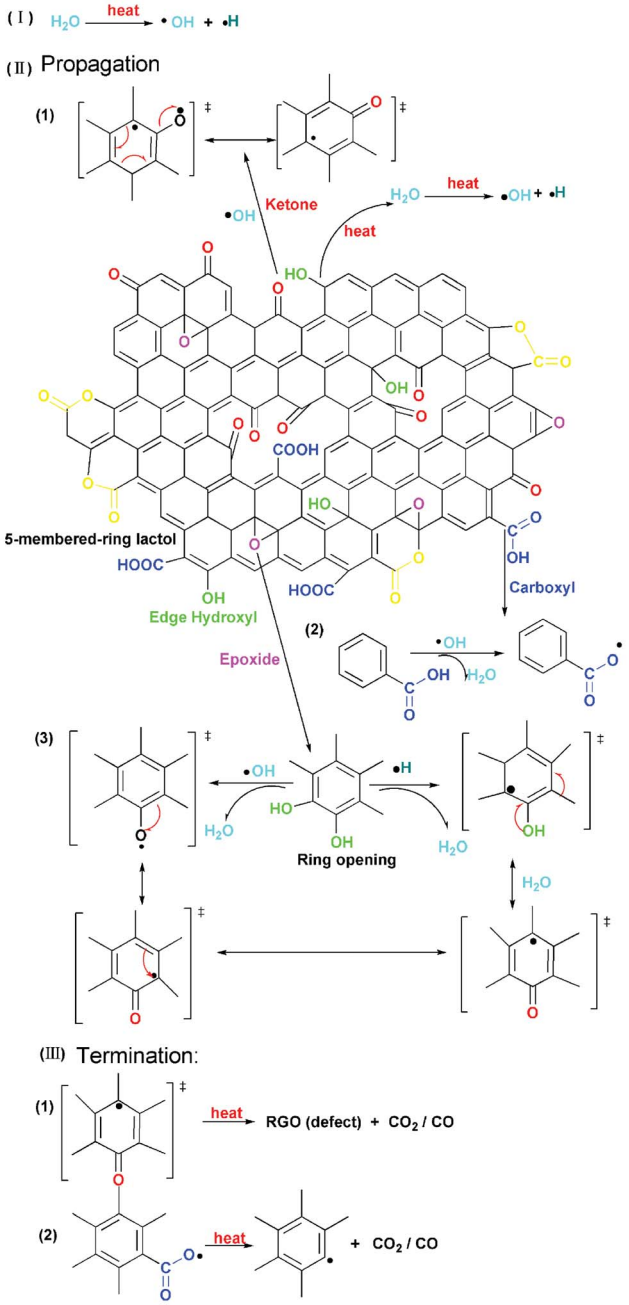

Scheme 5 Mechanism of the hydrothermal cutting of the O-RGO into GQDs.

‡ Schemes 3 and 4 only show the reactive sites in reduced graphene oxide.

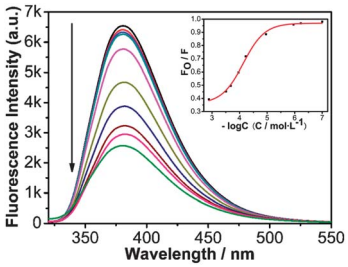

Fig. 11 Fluorescence emission spectra of GQD5 at pyrocatechol concentrations of 0, 10^{-7}, 5×10^{-7}, 10^{-6}, 10^{-5}, 5×10^{-5}, 10^{-4}, 10^{-3}, 5×10^{-3} mol L^{-1}. Inset: the fitted line plots of the GQDs-quenching system.

3.4. Potential applications of the GQDs

The fluorescence of GQDs is much more stable than some other fluoresceins with respect to photoirradiation. It is a benefit for applications of the fluorescence performance.

It was found that the fluorescence intensity of the GQDs decreased with increasing concentration of pyrocatechol. As shown in Fig. 11, different concentrations of pyrocatechol were added to a GQD solution and incubated for 25–30 min, and the intensity dramatically decreased (about 60%). The plot of the fluorescence intensity ratio (F_O/F) *vs.* the negative logarithm value of target concentration (–log C) showed the spectral response range being from 5.00×10^{-3} mol L^{-1} to 1.0×10^{-7} mol L^{-1} (inset of Fig. 11). There was no new peak with the addition of pyrocatechol. As the pyrocatechol was added, the fluorescence intensity of the GQDs decreased. However, after 5×10^{-3} mol L^{-1} the fluorescence emission peaks from 380 nm shift to 360 nm belonging to pyrocatechol. According to the above phenomenon, we proposed a possible interaction process of GQDs and pyrocatechol, and a plausible mechanism for quenching. The oxygen-containing groups in the GQDs not only made them have good water solubility and stability, but also enable noncovalent interactions with pyrocatechol through electrostatic interactions, π–π stacking or hydrogen bonding. There were several mechanisms for fluorescence quenching, such as energy transfer,[47,48] and charge transfer.[49] The energy transfer can account for the fluorescence quenching of the GQDs, because the fluorescence intensity was gradually quenched without peak-shifts with the addition of pyrocatechol (Fig. 11). The GQD-quenching approach could be used for the detection of pyrocatechol, with advantages such as less labor for synthesis of a fluorescent probe without auxiliary functionalization, high quenching efficiency and sensitivity. The GQD-quenching system provided a new general platform for the sensitive detection of pyrocatechol and wide applications in environmental, optoelectronic, biological labeling and biomedical fields.

4. Conclusions

In conclusion, we synthesized GQDs through a novel ozonation pre-oxide hydrothermal route, and studied the role that pH played on the fluorescence properties of the GQDs during the ozonation pre-oxide and hydrothermal procedures. The GQDs exhibited excellent stability and intensity with variable emission peaks taking ozone as an aggressive oxidant. Compared with mixed acid oxidant, ozonation processing is simple, efficient, low-cost, massively scalable and well-controlled. The oxygen-containing functional groups on the GQDs make them soluble in aqueous medium, facilitating further functionalization applications in fluorescent probes. In summary, using ozonation pre-oxide pH-dependent systems, not only provided a new route to control the properties of GQDs but also broadened the potential applications of the novel materials. A novel sensing platform for pyrocatechol based on the fluorescence quenching of the GQDs was proposed. Controllable GQDs with desired fluorescence will fulfil their promise for bulk applications.

Acknowledgements

We greatly appreciate the Natural Science Foundation of China (Grant 21075083) for supporting this work. We thank the Analytical & Testing Center, Sichuan University for HR-TEM measurements.

Notes and references

1 K. S. Novoselov, A. K. Geim, S. V. Morozov, D. Jiang, Y. Zhang, S. V. Dubonos, I. V. Grigorieva and A. A. Firsov, *Science*, 2004, **306**, 666.
2 D. Pan, S. Wang, B. Zhao, M. Wu, H. Zhang, Y. Wang and Z. Jiao, *Chem. Mater.*, 2009, **21**, 3136.
3 C. N. R. Rao, K. Biswas, K. S. Subrahmanyam and A. Govindaraj, *J. Mater. Chem.*, 2009, **19**, 2457.
4 Y. Liu, X. Dong and P. Chen, *Chem. Soc. Rev.*, 2012, **41**, 2283–2307.
5 Y. Dong, N. Zhou, X. Lin, J. Lin, Y. Chi and G. Chen, *Chem. Mater.*, 2010, **22**, 5895.
6 Y.-P. Sun, B. Zhou, Y. Lin, W. Wang, K. A. S. Fernando, P. Pathak, M. J. Meziani, B. A. Harruff, X. Wang, H. Wang, P. G. Luo, H. Yang, M. E. Kose, B. Chen, L. M. Veca and S.-Y. Xie, *J. Am. Chem. Soc.*, 2006, **128**, 7756.
7 Y. Li, Y. Hu, Y. Zhao, G. Shi, L. Deng, Y. Hou and L. Qu, *Adv. Mater.*, 2011, **23**, 776.
8 Y. Zhang, T. R. Nayak, H. Hong and W. Cai, *Nanoscale*, 2012, **4**, 3833.
9 M. Zhang, L. Bai, W. Shang, W. Xie, H. Ma, Y. Fu, D. Fang, H. Sun, L. Fan, M. Han, C. Liu and S. Yang, *J. Mater. Chem.*, 2012, **22**, 7461.
10 A. B. Bourlinos, A. Stassinopoulos, D. Anglos, R. Zboril, V. Georgakilas and E. P. Giannelis, *Chem. Mater.*, 2008, **20**, 4539.
11 W.-L. Yim and J. K. Johnson, *J. Phys. Chem. C*, 2009, **113**, 17636.
12 J. Lee, W. Song, S. S. Jang, J. D. Fortner, P. J. J. Alvarez, W. J. Cooper and J.-H. Kim, *Environ. Sci. Technol.*, 2010, **44**, 3786.
13 D. Pan, J. Zhang, Z. Li and M. Wu, *Adv. Mater.*, 2010, **22**, 734.
14 L. Yan, F. Zhao, S. Li, Z. Hu and Y. Zhao, *Nanoscale*, 2011, **3**, 362.
15 S. Zhu, J. Zhang, C. Qiao, S. Tang, Y. Li, W. Yuan, B. Li, L. Tian, F. Liu, R. Hu, H. Gao, H. Wei, H. Zhang, H. Sun and B. Yang, *Chem. Commun.*, 2011, **47**, 6858.
16 T. Sun, S. Fabris and S. Baroni, *J. Phys. Chem. C*, 2011, **115**, 4730.
17 X. Yan, X. Cui and L.-s. Li, *J. Am. Chem. Soc.*, 2010, **132**, 5944.
18 X. Yan, X. Cui, B. Li and L.-s. Li, *Nano Lett.*, 2010, **10**, 1869.
19 S. Zhu, J. Zhang, X. Liu, B. Li, X. Wang, S. Tang, Q. Meng, Y. Li, C. Shi, R. Hu and B. Yang, *RSC Adv.*, 2012, **2**, 2717.
20 G. Eda, Y.-Y. Lin, C. Mattevi, H. Yamaguchi, H.-A. Chen, I. S. Chen, C.-W. Chen and M. Chhowalla, *Adv. Mater.*, 2010, **22**, 505.
21 J.-L. Chen and X.-P. Yan, *J. Mater. Chem.*, 2010, **20**, 4328.
22 C. K. Chua, A. Ambrosi and M. Pumera, *J. Mater. Chem.*, 2012, **22**, 11054.
23 Z. Lin, Y. Yao, Z. Li, Y. Liu, Z. Li and C.-P. Wong, *J. Phys. Chem. C*, 2010, **114**, 14819.
24 C. Bosch-Navarro, E. Coronado, C. Marti-Gastaldo, J. F. Sanchez-Royo and M. G. Gomez, *Nanoscale*, 2012, **4**, 3977.
25 G. K. Ramesha and S. Sampath, *J. Phys. Chem. B*, 2009, **113**, 7985.
26 Y. Shao, J. Wang, M. Engelhard, C. Wang and Y. Lin, *J. Mater. Chem.*, 2010, **20**, 743.
27 P. Solís-Fernández, J. I. Paredes, S. Villar-Rodil, L. Guardia, M. J. Fernández-Merino, G. Dobrik, L. P. Biró, A. Martínez-Alonso and J. M. D. Tascón, *J. Phys. Chem. C*, 2011, **115**, 7956.

28 J. Liu, A. G. Rinzler, H. Dai, J. H. Hafner, R. K. Bradley, P. J. L. Boul, A. Lu, T. Iverson, K. Shelimov, C. B. Huffman, F. Rodriguez-Macias, Y.-S. Shon, T. R. Lee, D. T. Colbert and R. E. Smalley, *Science*, 1998, **280**, 1253.
29 J. D. Fortner, D. I. Kim, A. M. Boyd, J. C. Falkner, S. Moran, V. L. Colvin, J. B. Hughes and J. H. Kim, *Environ. Sci. Technol.*, 2007, **41**, 7497.
30 N. Leconte, J. l. Moser, P. Ordejón, H. Tao, A. l. Lherbier, A. Bachtold, F. Alsina, C. M. Sotomayor Torres, J.-C. Charlier and S. Roche, *ACS Nano*, 2010, **4**, 4033.
31 G. Lee, B. Lee, J. Kim and K. Cho, *J. Phys. Chem. C*, 2009, **113**, 14225.
32 K. P. Loh, Q. Bao, G. Eda and M. Chhowalla, *Nat. Chem.*, 2010, **2**, 1015.
33 L. M. Malard, M. A. Pimenta, G. Dresselhaus and M. S. Dresselhaus, *Phys. Rep.*, 2009, **473**, 51.
34 J. I. Paredes, S. Villar-Rodil, P. Solís-Fernández, A. Martínez-Alonso and J. M. D. Tascón, *Langmuir*, 2009, **25**, 5957.
35 L. R. Radovic and B. Bockrath, *J. Am. Chem. Soc.*, 2005, **127**, 5917.
36 M. L. Mueller, X. Yan, J. A. McGuire and L.-s. Li, *Nano Lett.*, 2010, **10**, 2679.
37 M. Grabolle, M. Spieles, V. Lesnyak, N. Gaponik, A. Eychmüller and U. Resch-Genger, *Anal. Chem.*, 2009, **81**, 6285.
38 Z. Luo, Y. Lu, L. A. Somers and A. T. C. Johnson, *J. Am. Chem. Soc.*, 2009, **131**, 898.
39 D. B. Mawhinney, V. Naumenko, A. Kuznetsova, J. T. Yates, J. Liu and R. E. Smalley, *J. Am. Chem. Soc.*, 2000, **122**, 2383.
40 M. Acik, G. Lee, C. Mattevi, A. Pirkle, R. M. Wallace, M. Chhowalla, K. Cho and Y. Chabal, *J. Phys. Chem. C*, 2011, **115**, 19761.
41 D. W. Boukhvalov and M. I. Katsnelson, *J. Am. Chem. Soc.*, 2008, **130**, 10697.
42 J. Staehelin and J. Hoigne, *Environ. Sci. Technol.*, 1982, **16**, 676.
43 H. Taube and W. C. Bray, *J. Am. Chem. Soc.*, 1940, **62**, 3357.
44 J. P. Pocostales, M. M. Sein, W. Knolle, C. von Sonntag and T. C. Schmidt, *Environ. Sci. Technol.*, 2010, **44**, 8248.
45 R. Flyunt, A. Leitzke, G. Mark, E. Mvula, E. Reisz, R. Schick and C. von Sonntag, *J. Phys. Chem. B*, 2003, **107**, 7242.
46 Z. Li, W. Zhang, Y. Luo, J. Yang and J. G. Hou, *J. Am. Chem. Soc.*, 2009, **131**, 6320.
47 H. Chang, L. Tang, Y. Wang, J. Jiang and J. Li, *Anal. Chem.*, 2010, **82**, 2341.
48 H. Dong, W. Gao, F. Yan, H. Ji and H. Ju, *Anal. Chem.*, 2010, **82**, 5511.
49 J.-L. Chen, X.-P. Yan, K. Meng and S.-F. Wang, *Anal. Chem.*, 2011, **83**, 8787.